J. of Basic Sciences, Cheju Nat'l Univ.
15(2), 19~26, 2002

기초과학연구 제주대학교
15(2), 19~26, 2002

Analysis of $^{12}C + ^{12}C$ Elastic Scattering at $E_{lab} = 360$ MeV Using the Second-Order Eikonal Model

Yong Joo Kim
Department of Physics and Research Institute for Basic Sciences, Cheju National University, Jeju 690-756

Dong Shik Kang
Department of Science Education, Cheju National University, Jeju 690-756

We analyze the $^{12}C + ^{12}C$ elastic scattering at $E_{lab} = 360$ MeV using the second-order eikonal model. The Fraunhöfer oscillations observed in the elastic scattering angular distributions could be explained due to the interference between the near- and far-side amplitudes. The elastic scattering pattern at large angles was dominated by the refraction of the far-side trajectories. The strongly real and a rather weakly imaginary optical potentials are required to describe the experimental data. The calculated effective potential shows drastic difference compared to ordinary potential in the small r values.

I. INTRODUCTION

In recent years, our understanding of the main features of the nuclear optical potential for light heavy-ions has advanced enormously. In the description of heavy-ion collisions, the strongly absorptive interaction is usually present. However, the data from the light heavy-ion system such as $^{12}C + ^{12}C$ and $^{16}O + ^{16}O$ show in their angular distributions refractive features which are interpreted as the dominance of contributions from the far side of the scattering center. The refractive phenomena seen in the light heavy-ion elastic scattering angular distributions uniquely determine the major features of the optical potentials.

A number of studies [1-8] have been made to describe the refractive scattering between the light heavy-ions. Shallow imaginary potentials are found to be essential to describe various sets of elastic scattering data for $^{12}C + ^{12}C$ and $^{16}O + ^{12}C$ systems at intermediate energies [1]. Brandan and McVoy [4] made a systematic study of the optical potentials for light heavy-ions. They made several interesting observations, especially on the characteristics of the ratios of the imaginary to real parts of the optical potentials and of the imaginary to real parts of the phase shifts. Ingemarsson *et al.* [3,6] have discussed the effects of the real potential on the absorption of light heavy-ion using the "effective potential".

The eikonal approximation [9,10] is widely used for the description of the heavy-ions elastic scattering. There are several efforts [11-13] to describe elastic scattering processes between heavy-ions within the framework of the eikonal approximation methods. Aguiar *et al.* [13] has discussed an extended eikonal model to the regime of low bombarding energies in heavy-ion collisions. In a recent paper [14], we have presented the first- and second-order corrections to the zeroth-order eikonal phase shifts for heavy-ion elastic scatterings based on Coulomb trajectories of colliding nuclei and it has been applied satisfactorily to the $^{16}O + ^{40}Ca$ and $^{16}O + ^{90}Zr$ systems at E_{lab}=1503 MeV. The elastic scattering cross sections of $^{12}C + ^{12}C$ system at E_{lab}= 240, 360 and 1016 MeV were analyzed [15] using the first-order non-eikonal phase shifts.

Buenerd *et al.* [16] have measured the elastic scattering of $^{12}C + ^{12}C$ system at $E_{lab} =$ 360 MeV and analyzed it using the optical model. In this paper, we reproduce the $^{12}C + ^{12}C$ elastic scattering $E_{lab} = 360$ MeV within the framework of the second-order eikonal model based on the Coulomb trajectories of colliding nuclei. The effects of real potential on the absorption are also discussed. In section II, we present the theory related with the second-order eikonal model. Section III contains the results and discussions for the second-order eikonal model analysis. Finally, concluding remarks are presented in section IV.

II. THEORY

The eikonal expansion of the phase shift function δ_L, as a power series in the strength of potential possessing spherical symmetry, in the distance of closest approach r_c representation is given in the following compact form [14]:

$$\delta_L(r_c) = \sum_{n=0}^{\infty} \delta_L^n(r_c), \tag{1}$$

where

$$\delta_L^n(r_c) = -\frac{k[\mu/(\hbar k)^2]^{n+1}}{(n+1)! {r_c}^{2n}} \left[{r_c}^2 \left(1 + r_c \frac{d}{dr_c}\right)\right]^n \int_0^{\infty} U^{n+1}(r)\, dz \tag{2}$$

with $r = \sqrt{r_c^2 + z^2}$. And μ is the reduced mass and the distance of closet approach r_c is given by

$$r_c = \frac{1}{k}\left\{\eta + \left[\eta^2 + (L+\frac{1}{2})^2\right]^{1/2}\right\} \tag{3}$$

with the Sommerfeld parameter η.

The zeroth-order term in this expansion is the ordinary Coulomb-modified eikonal phase shift function, while the corrections given by higher-order terms correspond to non-eikonal effects. The expressions for the first three terms in Eq.(2) are explicitly [14]

$$\delta_L^0(r_c) = -\frac{\mu}{\hbar^2 k}\int_0^{\infty} U(r)\, dz, \tag{4}$$

$$\delta_L^1(r_c) = -\frac{\mu^2}{2\hbar^4 k^3}\left(1 + r_c \frac{d}{dr_c}\right)\int_0^{\infty} U^2(r) dz, \tag{5}$$

$$\delta_L^2(r_c) = -\frac{\mu^3}{6\hbar^6 k^5}\left(3 + 5r_c\frac{d}{dr_c} + r_c^2\frac{d^2}{dr_c^2}\right) \int_0^{\infty} U^3(r)\, dz. \tag{6}$$

The first- and second-order eikonal correction terms of the phase shift, $\delta_L^1(r_c)$ and $\delta_L^2(r_c)$ in Eqs. (5) and (6) , can further be expressed as following

$$\delta_L^1(r_c) = -\frac{\mu^2}{\hbar^4 k^3}\int_0^{\infty}\left[U^2(r) + rU(r)\frac{dU(r)}{dr}\right] dz, \tag{7}$$

and

$$\delta_L^2(r_c) = -\frac{\mu^3}{6\hbar^6 k^5}\int_0^{\infty}\left[3r^2U^2\frac{d^2U}{dr^2} + 6r^2U(\frac{dU}{dr})^2 + 21rU^2\frac{dU}{dr} + 8U^3\right] dz. \tag{8}$$

The closed expression of the effective phase shift function including up to the second-order correction term may be written as

$$\delta_L(r_c) = -\frac{m}{\hbar^2 k}\int_0^{\infty} U_{\rm eff}(r)\, dz, \tag{9}$$

where $U_{\rm eff}(r)$ is the effective optical potential given by

$$U_{\rm eff}(r) = U\left\{1 + \frac{\mu}{\hbar^2 k^2}U_1 + \frac{\mu^2}{6\hbar^4 k^4}U_2\right\} \tag{10}$$

with

$$U_1 = U + r\frac{dU}{dr}, \tag{11}$$

$$U_2 = 3r^2U\frac{d^2U}{dr^2} + 6r^2(\frac{dU}{dr})^2 + 21rU\frac{dU}{dr} + 8U^2. \tag{12}$$

We can see that the phase shift calculation including non-eikonal corrections up to the second-order is equivalent to a zeroth-order calculation with effective potential $U_{\rm eff}(r)$. By taking $U(r)$ as the optical Woods-Saxon forms given by

$$U(r) = -\frac{V_0}{1 + e^{(r-R_v)/a_v}} - i\frac{W_0}{1 + e^{(r-R_w)/a_w}}, \tag{13}$$

with $R_{v,w} = r_{v,w}(A_1^{1/3} + A_2^{1/3})$, we can use the phase shifts, Eqs.(4)-(6) in the general expression for the elastic scattering amplitude. The elastic scattering cross section is then obtained from the scattering amplitude

$$f(\theta) = f_{\rm R}(\theta) + \frac{1}{ik}\sum_{L=0}^{\infty}(L+\frac{1}{2})\exp(2i\sigma_L) (S_L^{\rm N} - 1)P_l(\cos\theta) \tag{14}$$

where $f_{\rm R}(\theta)$ is the usual Rutherford scattering amplitude, k is the wave number and σ_L the Coulomb phase shifts. The nuclear S-matrix elements S_L^N can be expressed in terms of nuclear phase shifts δ_L given by

$$S_L^N = \exp(2i\delta_L). \tag{15}$$

TABLE I: Parameters of the fitted Woods-Saxon potential from the second-order eikonal model for $^{12}C + ^{12}C$ system at $E_{lab} = 360$ MeV.

V_o (MeV)	r_v (fm)	a_v (fm)	W_o (MeV)	r_w (fm)	a_w (fm)
188	0.661	0.816	35.3	0.980	0.706

TABLE II: Strong absorption distances ($R_{1/2}$), reaction cross sections (σ_R) and χ^2/N values from the second-order eikonal model analysis for $^{12}C + ^{12}C$ system at $E_{lab} = 360$ MeV. 10 % error bars are adopted to obtain χ^2/N values.

$R_{1/2}$ (fm)	σ'_R (mb)	σ_R (mb)	χ^2/N		
			δ_0	$\delta_0 + \delta_1$	$\delta_0 + \delta_1 + \delta_2$
6.19	1204	1245	10.71	3.68	2.68

III. RESULTS AND DISCUSSIONS

The measured angular distribution [16] for $^{12}C + ^{12}C$ elastic scatterings at E_{lab}= 360 MeV is given as the ratio of the experimental cross section to the Mott cross section. This data exhibit a typical Fraunhöfer diffraction pattern at small scattering angles followed by an exponential fall-off at large angles. The analysis has been carried out using the second-order eikonal model formalism based on Coulomb trajectories of colliding nuclei. Woods-Saxon potential parameters were adjusted to obtain the least χ^2/N fit to the elastic scattering data. The potential parameter sets obtained from second-order eikonal model fit to the data at 360 MeV are listed in table I. The calculated results of the differential cross sections for the elastic scattering of $^{12}C + ^{12}C$ system at E_{lab}= 360 MeV are depicted in Fig. 1 together with the observed data [16]. In Fig.1, the dotted curve is the result for the zeroth-order eikonal phase shift, while the dashed and solid curves are the results for the first- and second-order corrections. As seen in this figure, the differences between the dotted and dashed and solid curves are substantial when compared to the experimental results. The second-order eikonal model reproduce the characteristic refractive pattern observed experimentally. Three calculated angular distributions are nearly identical at forward angles but are qualitatively different at large angles. As a whole, our calculations lead to reasonable predictions over the whole angular range for the elastic scattering data in the $^{12}C + ^{12}C$ system at E_{lab}= 360 MeV. The reasonable χ^2/N value in the second-order eikonal model is also obtained as listed in table II.

In Figure 2, we plot the transmission function T_L as a function of angular momentum L, along with the partial reaction cross section. As shown in Fig. 2(a), the lower partial waves are totally absorbed and the T_L is decreased very rapidly in a narrow localized angular momenta zone. The T_L distribution can be used to define the strong absorption distance $R_{1/2}$, a quantity which characterizes the system with respect to strong absorption. The $R_{1/2}$ value in table II is the distance of closest approach for which $T_L = \frac{1}{2}$. For internuclear distances smaller than $R_{1/2}$ the absorption dominates, whereas for values larger than $R_{1/2}$ partial waves are mostly deflected in the elastic channel. We can see that the strong absorption distance provides

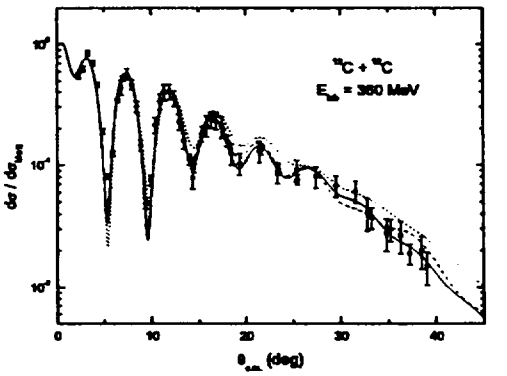

FIG. 1: Elastic scattering angular distributions for $^{12}C + ^{12}C$ system at $E_{lab} = 360$ MeV. The solid circles denote the observed data taken from Buenerd *et al.* [16]. The dotted, dashed and solid curves are the calculated results for zeroth-, first- and second-order eikonal corrections, respectively.

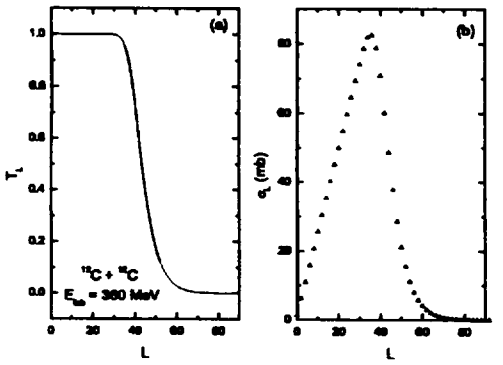

FIG. 2: (a) Transmission function T_L and (b) partial reaction cross section σ_L from the second-order eikonal model for $^{12}C + ^{12}C$ system at E_{lab} = 360 MeV.

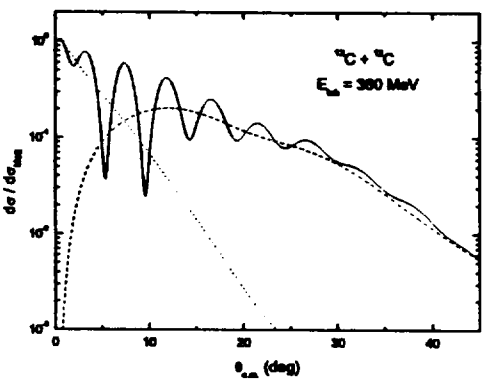

FIG. 3: Differential cross sections (solid curves), near-side contributions (dotted curves), and far-side contributions (dashed curves) following the Fuller's formalism [17] from the second-order eikonal model.

a good measurement of reaction cross section in terms of $\sigma_R = \pi R_{1/2}^2$. We found in Fig. 2(b) that the value of the partial wave reaction cross section increases linearly up to L = 36. Beyond this L value, the partial reaction cross section decrease quardratically.

More realistic insight into the diffractive and refractive phenomena can be provided by the representation of the elastic scattering amplitude in terms of the near-side and far-side components. The near-side amplitude represents contributions from waves deflected to the direction of θ on the near-side of the scattering center and the far-side amplitude represents contributions from waves traveling from the opposite, far side of the scattering center to the same angle θ. The near- and far-side decompositions of the scattering amplitudes with the second-order eikonal model for $^{12}C + ^{12}C$ system at E_{lab}= 360 MeV, were performed by following the Fuller's formalism [17]. The contribution of the near- and far-side components to the elastic scattering cross sections is shown in Fig.3 along with the differential cross sections. The differential cross section is not just a sum of the near- and far-side cross sections but contains the interference between the near- and far-side amplitudes as shown in Fig.3. At small angles the near-side amplitude dominates, corresponding to the positive-angle trajectories. At these angles the far-side contribution is very small, but increases with the angle whereas the near-side amplitude decreases. The Fraunhöfer diffraction pattern at intermediate angles where two amplitudes are of comparable magnitudes, is due to the interferences between the near- and far-side contributions. The magnitudes of the near- and far-side contributions are equal, crossing point, at $\theta = 7.3°$. However, the elastic scattering pattern at large angles is dominated by the refraction of the far-side trajectories and carries important information on the interaction potential between the heavy-ions.

In order to illustrate the effect of higher-order non-eikonal corrections, we plotted in Fig.4 both the real and imaginary parts up to the second-order effective potential $U_{eff}(r)$ given in Eq.(10). As shown in figure 4(a), drastic changes in real parts of effective potential was noticed, especially in the central region of the nucleus. It is seen that the effective potential of second-order eikonal model increases the depth of the real part of the optical potential in small r values compared to one of the first-order eikonal model. While in case of imaginary potential, there is a dramatic differences between three potential as shown in figure 4(b). In the ordinary eikonal model, the shape of imaginary poten-

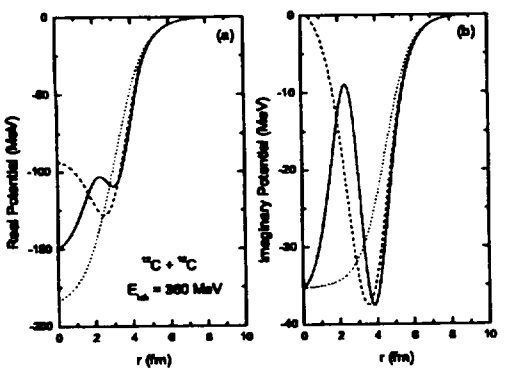

FIG. 4: (a) Real and (b) imaginary parts of effective optical potentials for $^{12}C + ^{12}C$ system at E_{lab} = 360 MeV. The dotted, dashed and solid curves are the calculated results for zeroth-, first- and second-order eikonal corrections, respectively.

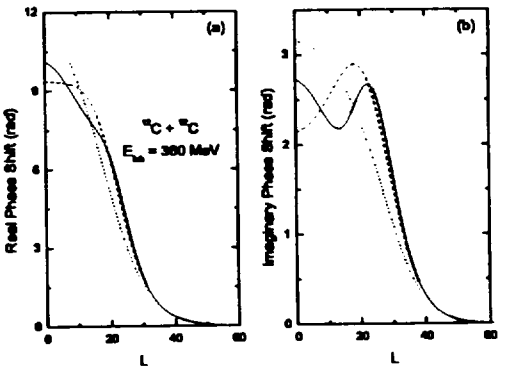

FIG. 5: (a) Real and (b) imaginary parts of effective phase shifts for $^{12}C + ^{12}C$ system at E_{lab} = 360 MeV. The dotted, dashed and solid curves are the calculated results for zeroth-, first- and second-order eikonal corrections, respectively.

tial should not be affected by the real part. In the first-order eikonal model, the effective imaginary potential depends on the product of the real and imaginary potentials and their derivatives. The result of eikonal correction increases the imaginary potential at small values of r. However, in second-order corrections this simple picture is no longer valid since the imaginary part is rather a complicated function of both the real and imaginary parts of optical potential. The effective imaginary potential displays pronounced minimum and maximum values. The pronounced minimum value of imaginary potential for the second-order eikonal model displaced towards the right as compared to value of the first-order one, while its depths were almost equal.

Figure 5 shows the angular momentum dependence of real and imaginary parts of zeroth-, first- and second-order eikonal phase shift. The effective potentials in the small r regions are also reflected in the phase shift function through the inverse eikonal relationship. The real phase shifts of first- and second-order corrections are shifted toward the right compared to one of zeroth-order eikonal phase at the large values of L. However, we can also find the dramatic variations of imaginary phase shifts for the non-eikonal corrections, as expected. Zeroth-order imaginary eikonal phase shift decrease monotonically as L increase. On the other hand, first-order effective phase shift shows one broad maximum near $L = 18$. While the second-order eikonal one exhibit somewhat oscillatory structure. We can see in the second-order eikonal model that an absorption of partial waves for large L increases, while the absorption decreases until to the broad minimum and increases again at small L values. The strong absorption in the nuclear surface plays a dominant role to the scattering amplitude and thus to the characteristic diffraction pattern of the angular distribution. The large-angle behavior is sensitive to the details of the real optical potential over a wide radial region from the nuclear surface towards the interior.

Figure 6 show the ratio of the imaginary to real parts of the optical potentials and phase shifts, respectively. For small r values, imaginary potential of second-order eikonal model is very weak compared to real potential over the small r range. Such a potential feature is responsible for large angle cross sections. So to speak, the strong real potential make it possible to deflect internal trajectories to large negative angles. We can see that the refractive part, dominated by the far-side com-

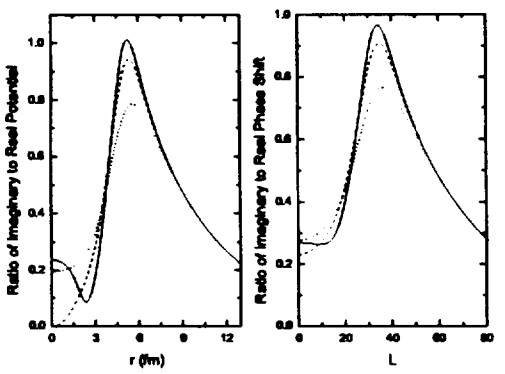

FIG. 6: Ratio of imaginary to real parts of (a) optical potentials and (b) phase shifts for ^{12}C + ^{12}C system at E_{lab} = 360 MeV. The dotted, dashed and solid curves are the calculated results for zeroth-, first- and second-order eikonal corrections, respectively.

ponent of the scattering amplitude, is related with the deep real heavy-ion optical potential. In the large r ranges, both real and imaginary potentials have exponential tails. The peak values of the potential ratios increase as the orders of non-eikonal corrections are higher. Phase shift ratio show a similar structure with the potential ratio, as shown in Fig. 6(b). As expected, the imaginary phase is small in the small L values, compared to real one due to characteristics of effective potential. Such a behavior of the phase shift in the small L ranges is responsible for large angle cross sections which are directly related with the deep real part of optical potential, and corresponding trajectories are penetrating the nuclear interior. Similar to potential ratio, the pronounced maximum of phase shift ratio is existed. The height of peak values of phase shift ratio increase as the higher-order non-eikonal corrections are increase. Both real and imaginary potentials have exponential tails in the large L ranges.

IV. CONCLUDING REMARKS

In this paper, we have analyzed the elastic scattering of ^{12}C + ^{12}C systems at E_{lab}= 360 MeV using the second-order eikonal model based on the Coulomb trajectories of colliding nuclei. The calculated result leads to a reasonably good agreements with observed data. We can see that the strong absorption distance provides a good measurement of reaction cross section in terms of $\sigma_R' = \pi R_{1/2}^2$. We have also found that the value of the partial wave reaction cross section increases linearly up to $L = 36$. Beyond this L value, the partial reaction cross section decrease quardratically. Through near- and far-side decompositions of the cross section for ^{12}C + ^{12}C system, the Fraunhöfer oscillations at intermediate angles are due to the interference between the near- and far-side amplitude. The elastic scattering pattern at large angles was dominated by the refraction of the far-side trajectories.

We found that the strongly real and a rather weakly imaginary optical potentials are required to describe the experimental data and this potential features make it possible to interpenetrate each other between the projectile and target nuclei. The effective imaginary potential in second-order eikonal model displays pronounced minimum and maximum values. The pronounced minimum value of imaginary potential for the second-order eikonal model displaced towards the right as compared to value of the first-order one, while its depths were almost equal. The first-order effective imaginary phase shift shows one broad maximum near $L = 18$. On the other hand, the second-order eikonal one exhibit somewhat oscillatory structure. We can see in the second-order eikonal model that an absorption of partial waves for large L increases, while the absorption decreases until to the broad minimum and increases again at small L values. Phase shift ratio show a similar structure with the potential ratio. The height of peak values of potential ratio and phase shift ratio increase as the orders of non-eikonal correction are increase. The imaginary potential of second-order eikonal model is very weak compared to real potential over the small r range. Such a potential feature is responsible for large angle cross sections. The strong real potential make it possible to deflect internal trajectories to large negative angles. As a result the projectile ion can penetrate the nuclear surface barrier of

the target, and the cross section becomes sensitive to the value of the real potential at the small r values.

[1] M. E. Brandan, Phys. Rev. Lett. **60**, 784 (1988).

[2] E. Stiliaris, H. G. Bohlen, P. Fröbrich, B. Gebauer, D. Kolbert, W. von Oertzen, M. Wilpert and Th. Wilpert, Phys. Lett. **223**, 291 (1989).

[3] A. Ingemarsson and G. Fäldt, Phys. Rev. **C48**, R507 (1993).

[4] M. E. Brandan, H. Chehime and K. W. McVoy, Phys. Rev. **C55**, 1353 (1997).

[5] S. M. Eliseev and K. M. Hanna, Phys. Rev. **C56**, 554 (1997).

[6] A. Ingemarsson, Phys. Rev. **C56**, 950 (1997).

[7] A. A. Olgloblin, Yu. A. Glukhov, W. H. Trzaska, A. S. Dem'yanova, S. A. Goncharov, R. Julin, S. V. Klebnikov, M. Mutterer, M. V. Rozhkov, V. P. Rudakov, G. P. Tiorin, Dao T. Khoa, and G. R. Satchler, Phys. Rev. **C62**, 044601 (2000).

[8] Dao T. Khoa, W. von Oertzen, H. G. Bohlen, F. Nuoffer, Nucl. Phys. **A672** 387 (2000).

[9] T. W. Donnelly, J. Dubach and J. D. Walecka, Nucl. Phys. Nucl. Phys. **A232**, 355 (1974).

[10] J. Knoll and R. Schaeffer, Ann. Phys. (N.Y.) **97**, 307 (1976).

[11] R. da Silveira and Ch. Leclercq-Willain, J. Phys. **G13**, 149 (1987).

[12] F. Carstoiu and R. J. Lombard, Phys. Rev. **C48** 830 (1993).

[13] C. E. Aguiar, F. Zardi, and A. Vitturi, Phys. Rev. **C56**, 1511 (1997).

[14] M. H. Cha and Y. J. Kim, Phys. Rev. **C51**, 212 (1995).

[15] Y. J. Kim and M. H. Cha, Int. J. Mod. Phys. **E9**, 67 (2000).

[16] M. Buenerd, A. Lounis, J. Chauvin, D. Lebrun, P. Martin, G. Duhamel, J. C. Gondrand, and P. De Saintignon, Nucl. Phys. **A424**, 313 (1984).

[17] R. C. Fuller, Phys. Rev. **C12**, 1561 (1975).

제 2 차 Eikonal 모형을 이용한 E_{lab} = 360 MeV 에서의 ^{12}C + ^{12}C 탄성산란 분석

김용주

제주대학교 물리학과 · 기초과학연구소, 제주 690-756

강동식

제주대학교 과학교육과, 제주 690-756

제2차 Eikonal 모형을 이용하여 E_{lab} = 360 MeV 에서의 ^{12}C + ^{12}C 탄성산란을 분석하였다. 탄성산란 각분포에서 관측되는 Fraunhöfer 진동은 근측과 원측 진폭들의 간섭현상으로 설명할 수 있었다. 큰 산란각에서 탄성산란 퍼턴은 원측궤적들의 굴절에 의해 지배를 받음을 알 수 있었다. 실험 데이터를 기술하기 위해서는 강한 실수 퍼텐셜과 비교적 약한 허수 퍼텐셜이 요구되었다. 계산된 유효 퍼텐셜은 작은 반경영역에서 보통의 퍼텐셜과 큰 차이가 있었다.